Reduction of peak acoustic pressure and shaping of heated region by use of multifoci sonications in MR-guided high-intensity focused ultrasound mediated mild hyperthermia

Ari Partanen
Center for Interventional Oncology, Clinical Center, National Cancer Institute, National Institutes of Health, Bethesda, Maryland 20892; Department of Physics, University of Helsinki, Helsinki 00014, Finland; and Philips Healthcare, Cleveland, Ohio 44143

Matti Tillander
Philips Medical Systems, Vantaa, Uusimaa 01510, Finland

Pavel S. Yarmolenko
Center for Interventional Oncology, Clinical Center, National Cancer Institute, National Institutes of Health, Bethesda, Maryland 20892 and Department of Biomedical Engineering, Duke University, Durham, North Carolina 27708

Bradford J. Wood and Matthew R. Dreher
Center for Interventional Oncology, Clinical Center, National Cancer Institute, National Institutes of Health, Bethesda, Maryland 20892

Max O. Köhler[a)]
Philips Medical Systems, Vantaa, Uusimaa 01510, Finland

(Received 20 June 2012; revised 5 October 2012; accepted for publication 6 November 2012; published 19 December 2012)

Purpose: Ablative hyperthermia (>55 °C) has been used as a definitive treatment for accessible solid tumors not amenable to surgery, whereas mild hyperthermia (40–45 °C) has been shown effective as an adjuvant for both radiotherapy and chemotherapy. An optimal mild hyperthermia treatment is spatially accurate, with precise and homogeneous heating limited to the target region while also limiting the likelihood of unwanted thermal or mechanical bioeffects (tissue damage, vascular shut-off). Magnetic resonance imaging-guided high-intensity focused ultrasound (MR-HIFU) can noninvasively heat solid tumors under image-guidance. In a mild hyperthermia setting, a sonication approach utilizing multiple concurrent foci may provide the benefit of reducing acoustic pressure in the focal region (leading to reduced or no mechanical effects), while providing better control over the heating. The objective of this study was to design, implement, and characterize a multifoci sonication approach in combination with a mild hyperthermia heating algorithm, and compare it to the more conventional method of electronically sweeping a single focus.

Methods: Simulations (acoustic and thermal) and measurements (acoustic, with needle hydrophone) were performed. In addition, heating performance of multifoci and single focus sonications was compared using a clinical MR-HIFU platform in a phantom (target = 4–16 mm), in normal rabbit thigh muscle (target = 8 mm), and in a Vx2 tumor (target = 8 mm). A binary control algorithm was used for real-time mild hyperthermia feedback control (target range = 40.5–41 °C). Data were analyzed for peak acoustic pressure and intensity, heating energy efficiency, temperature accuracy (mean), homogeneity of heating (standard deviation [SD], T10 and T90), diameter and length of the heated region, and thermal dose (CEM_{43}).

Results: Compared to the single focus approach, multifoci sonications showed significantly lower (67% reduction) peak acoustic pressures in simulations and hydrophone measurements. In a rabbit Vx2 tumor, both single focus and multifoci heating approaches were accurate (mean = 40.82±0.12 °C [single] and 40.70±0.09 °C [multi]) and precise (standard deviation = 0.65±0.05 °C [single] and 0.64±0.04 °C [multi]), producing homogeneous heating ($T_{10–90}$ = 1.62 °C [single] and 1.41 °C [multi]). Heated regions were significantly shorter in the beam path direction (35% reduction, $p < 0.05$, Tukey) for multifoci sonications, i.e., resulting in an aspect ratio closer to one. Energy efficiency was lower for the multifoci approach. Similar results were achieved in phantom and rabbit muscle heating experiments.

Conclusions: A multifoci sonication approach was combined with a mild hyperthermia heating algorithm, and implemented on a clinical MR-HIFU platform. This approach resulted in accurate and precise heating within the targeted region with significantly lower acoustic pressures and spatially more confined heating in the beam path direction compared to the single focus sonication method.

The reduction in acoustic pressure and improvement in spatial control suggest that multifoci heating is a useful tool in mild hyperthermia applications for clinical oncology. © *2013 American Association of Physicists in Medicine*. [http://dx.doi.org/10.1118/1.4769116]

Key words: MR-HIFU, thermotherapy, multifoci, mild hyperthermia

I. INTRODUCTION

Hyperthermia has been used extensively and successfully in the treatment of solid tumors. Often when surgery is not indicated, ablative hyperthermia (>55 °C for 20 s–15 min) has been used as a definitive treatment for certain solid tumors with impressive efficacy,[1] whereas mild hyperthermia (40–45 °C for up to 1 h) has been used as an adjuvant with both chemotherapy and radiation therapy.[2–4] While the primary goal of ablative hyperthermia is to ensure cancer cell death, the beneficial effects of mild hyperthermia lie in its ability to improve the effectiveness of other treatments through sensitization by modifying both the physiology and biology of cancer.[5,6] Mild hyperthermia may provide improved tissue perfusion and oxygenation, inhibit homologous recombination,[7] improve delivery of chemotherapy and potentiate its cytotoxic effects,[2] as well as augment immune response.[8] Culmination of these effects has great potential to improve outcomes for cancer patients who often receive radio- and chemotherapy. This benefit could be realized through the simple addition of a mild hyperthermia treatment to the normal course of therapy.[3,4,9]

Widespread use of mild hyperthermia has been limited to date by applicators with insufficient performance and which are ill-suited for current clinical workflow. Traditional applicators include radiofrequency,[10,11] microwave,[12,13] hot water baths,[14] lasers,[15,16] and magnetic fluids.[17,18] These suffer from drawbacks such as the invasive nature of applicators, limited and superficial heating, formation of hot and cool spots, inaccurate or spatially uneven heating, and lack of spatiotemporal feedback control.

Magnetic resonance imaging-guided high-intensity focused ultrasound (MR-HIFU) may address the challenges faced by the more traditional devices through a combination of anatomic and temperature imaging capabilities of magnetic resonance imaging (MRI) with highly localized and noninvasive heating of HIFU, yielding excellent spatiotemporal control and thermal accuracy. Real-time temperature monitoring with MRI is commonly achieved with the water proton resonance frequency shift (PRFS) method,[19] which relies on the linear dependence of PRFS on temperature change [standard deviation (SD) < 1 °C (Ref. 20)]. In the mild hyperthermic range, this linear relationship is valid in all nonadipose tissues.[20,21]

Application of HIFU can result in both thermal and nonthermal (often known as mechanical) bioeffects, both of which arise from a complex interaction of propagating ultrasound waves with tissue.[22] Importantly, HIFU bioeffects can be manipulated and/or controlled by device output power, ultrasound frequency, duty cycle, sonication duration, and focal spot characteristics. The thermal effects are due to ultrasound absorption and conversion to heat through vibrational excitation of tissue, leading to rapid, highly localized temperature elevation. The mechanical bioeffects that are unique to HIFU include acoustic radiation forces and acoustic cavitation. Radiation forces may lead to local tissue displacement, shear strain, and streaming.[23] Cavitation effects are mediated by bubble activity—collapsing or oscillating bubbles can lead to locally induced stress and high energy release, possibly resulting in and enhancing thermal coagulation and necrosis.[24] The ultrasound mechanical effects may be exploited to improve ablation efficiency,[25,26] or to improve drug delivery with or without the use of microbubbles.[27,28]

The effects of HIFU on tissue are highly dependent on the acoustic pressure in the focal region, with different mechanisms of HIFU energy propagation dominating at high and low acoustic pressures. When operating at low acoustic pressures, the acoustic field is predominantly linear, the waves have harmonic shape, and acoustic intensity is proportional to the pressure squared. At higher acoustic pressure levels, the peak negative (rarefaction) pressure correlates well with the onset of cavitation effects,[24,29,30] and nonlinear wave propagation leads to generation of higher harmonics, asymmetric distortion of the pressure waveforms, and ultimately, to formation of steep shock fronts.[31] The nonlinear broadening of the spectrum to higher frequencies and the formation of shocks can significantly increase local absorption of acoustic energy, especially in the focal region, thereby drastically increasing the heating rate.[32–34] The unpredictable nature of nonlinear acoustic propagation and mechanical bioeffects raises potential concerns for clinical translation into a diverse patient population. Thus, regulatory implications for HIFU mild hyperthermia applicators may be more favorable for low acoustic intensities and pressures.

Phased-array transducers in combination with appropriate driving electronics enable the creation of a desired focal pattern by offering fast temporal displacement of a single focus, or the generation of multiple simultaneous foci associated with low levels of secondary maxima.[35–39] For thermal ablation (T > 55 °C), it is desirable to achieve a rapid, highly localized temperature rise in the target region in order to limit undesired temperature elevation in surrounding tissues. Desirable properties for ablation include high energy efficiency of the heating, as well as steep temperature gradients for improved lesion delineation. Provided the ablation is complete and continuous, temperature uniformity within the target region is of little interest. Consequently, sweeping a single high-intensity focus to increase the ablation volume has shown benefit for ablation.[39–41] Low-level cavitation and shock wave formation near the focus, induced by high pressures, may even be beneficial in further improving ablation heating efficiency, as long as collateral damage to surrounding tissues can be

avoided. The requirements placed upon the heating strategy are almost opposite for mild hyperthermia: mechanical effects may be a substantial problem as the goal is merely to elevate local temperature while avoiding direct tissue damage. Heating uniformity is also of greater importance for mild hyperthermia, as this therapy intends to achieve similar bioeffects throughout the target volume.

However, the low target temperature range of mild hyperthermia suggests that thermal damage to the skin and near field is unlikely; thus, heating efficiency is consequently of secondary interest. Multifoci patterns, which distribute the acoustic pressure over a larger area, possibly at the cost of slightly inferior heating efficiency and less well-defined treatment borders, may thus be beneficial for mild hyperthermia treatments. Both single focus and multifoci approaches may be used to manipulate or to prescribe the shape of a heated volume. However, multifoci sonications may allow for lower instantaneous pressures and intensities.

The objective of this study was to develop a multifoci sonication approach for mild hyperthermia with MR-HIFU in order to mitigate the possible risks associated with high instantaneous pressures, and to obtain a homogeneous temperature distribution in the target region. Transducer element amplitudes and phases were manipulated *in silico* to obtain an optimal focus pattern that was evaluated with simulations and then validated with hydrophone measurements. This multifoci approach was implemented on a clinical MR-HIFU system in conjunction with volumetric mild hyperthermia binary feedback control.[42] The performance of this sonication approach was evaluated in comparison to electronic sweeping of a single focus in both *in vitro* and *in vivo* MR-HIFU experiments.

II. MATERIALS AND METHODS

II.A. Generation of sonications patterns

Single-focus sonication trajectories were performed as described by Köhler *et al.*,[39] whereas multifoci patterns were generated based on the work of Ebbini and Cain[36] and Fan and Hynynen.[37]

Briefly, the complex pressure at a point in the acoustic field can be written as

$$p(\boldsymbol{r}) = \frac{j\rho ck}{2\pi}\int_{S'} u(\boldsymbol{r}')\frac{\exp(-jk\left|\boldsymbol{r}-\boldsymbol{r}'\right|)}{|\boldsymbol{r}-\boldsymbol{r}'|}dS',$$

where $j=\sqrt{-1}$, ρ is the density, c is the speed of sound, k is the wavenumber, S' is the surface of the source, u is the normal velocity of the source surface, and $\boldsymbol{r}$ and $\boldsymbol{r}'$ are the observation and source points, respectively.

For a phased-array transducer with N elements, the pressure as given in M control points at position $\boldsymbol{r}=\boldsymbol{r_m}$ with $m=1,2,\ldots,M$ can be written as

$$p(\boldsymbol{r_m}) = \frac{j\rho ck}{2\pi}\sum_{n=1}^{N} u_n \int_{S'_n}\frac{\exp(-jk\left|\boldsymbol{r_m}-\boldsymbol{r'_n}\right|)}{\left|\boldsymbol{r_m}-\boldsymbol{r'_n}\right|}dS'_n.$$

This equation can be further written into matrix form according to

$$\boldsymbol{Hu}=\boldsymbol{p},$$

where $\boldsymbol{u}=[u_1,u_2,\ldots,u_N]$ and $\boldsymbol{p}=[p(\boldsymbol{r}_1),p(\boldsymbol{r}_2),\ldots,p(\boldsymbol{r}_M)]$ and $\boldsymbol{H}$ is the forward propagator

$$H(m,n) = \frac{j\rho ck}{2\pi}\sum_{n=1}^{N}\int_{S'_n}\frac{\exp(-jk\left|\boldsymbol{r_m}-\boldsymbol{r'_n}\right|)}{\left|\boldsymbol{r_m}-\boldsymbol{r'_n}\right|}dS'_n.$$

Using the matrix formulation above, one can then solve for the driving amplitude and phase of the N transducer elements that is required to generate the desired pressure amplitude and phase in the M control points. Normally, when $M<N$, and when $\boldsymbol{H}$ has full rank, the minimum-norm solution to the matrix problem above is given by

$$\widehat{\boldsymbol{u}}=\boldsymbol{H}^{*'}(\boldsymbol{H}\boldsymbol{H}^{*'})^{-1}\boldsymbol{p},$$

where $\boldsymbol{H}^{*'}$ is the conjugate transpose. If a certain number of simultaneous foci are then desired, they can be defined as control points with a certain pressure amplitude and phase at a prescribed position $\boldsymbol{r_m}$.

In this study, the control points for the generation of the multifoci patterns were chosen to have equal pressure magnitude. The phase at control points was chosen in order to minimize constructive interference outside of the focal plane and thus limit and shape the heated volume in the beam axis direction. To achieve this, simulations were performed by varying the phase at each control point, and results (data not shown) were rated based on temperature uniformity, acoustic pressure, and length of heated volume in the beam axis direction. From the set of solutions, a phase increment of 180° between neighboring control points best addressed the abovementioned criteria, and was subsequently used in all experiments.

Both single focus and multifoci volumetric sonications were performed using circular subtrajectories of size 4, 8, 12, and 16 mm in diameter.[39,43] In the single focus sonication approach, subtrajectories were sonicated by temporally sweeping a single focus through 8, 16, 24, and 32 discrete sonication locations (sonicated for 50 ms/location) for the 4, 8, 12, and 16 mm subtrajectories, respectively. These sonication locations were evenly distributed along the circular subtrajectories perpendicularly to the beam path.[39] The same sonication locations were also used in the case of the multifoci sonications although in this case all locations were sonicated simultaneously rather than sequentially.

II.B. Acoustic and thermal simulations

Acoustic and thermal simulations were performed in MATLAB 7.0 (MathWorks, Natick, MA) in order to evaluate acoustic pressures as well as mild hyperthermia heating performance and energy efficiency for both single focus and multifoci sonications.

Acoustic simulations utilized the Rayleigh–Sommerfeld integral[44] with a resolution of 0.3 × 0.08 × 0.08 mm^3 and field-of-view (FOV) of 72 (beam axis) × 32 × 32 mm^3. Simulations were done using a two-layer model (water and muscle) with the target plane being placed at a depth of 20 mm within the muscle to mimic the animal experiments. The

TABLE I. Tissue parameters used for acoustic and thermal simulations.

Parameter	Value
Speed of sound, c (m/s)	1540
Density (tissue), σ_t (kg/m^3)	1020
Thermal conductivity, k (W/m/K)	0.55
Specific heat capacity (tissue), c_t (J/kg/K)	3600
Attenuation, α (Np/m)	8.5
Perfusion rate, w (ml/ml/s)	0.002
Density (blood), σ_b (kg/m^3)	1050
Specific heat capacity (blood), c_b (J/kg/K)	3770

pressure amplitude of the transducer elements in the multifoci case was scaled so as to provide the same total acoustic power as the single focus sonication on the transducer surface. Tissue parameters were obtained from Goss *et al.*, Duck, and Valvano,[45–47] and are provided in Table I.

Thermal simulations, based on the Pennes' bioheat transfer equation,[48] were performed for the 8 mm diameter sonications (single focus and multifoci) using a Fourier-based approach[49] and assuming the temperature of the flowing blood to be equal to the core body temperature. The simulated sonications consisted of three stages: heat-up of the 4 mm diameter subtrajectory (60 s), heat-up of the 8 mm subtrajectory (120 s), and the maintenance stage of the 8 mm subtrajectory (7 min), resulting in 10 min of total heating. The acoustic power for each stage was adjusted so as to reach a minimum temperature of 40.5 °C within the given time in a volume defined by a 4 mm thick disk with diameter equal to the sonicated subtrajectory and centered on the beam axis with offset of 2 mm toward the near field. Volumetric heating efficiency was calculated as the ratio of volume heated over 40.5 °C to the total required energy per heating stage.

II.C. Hydrophone measurements

In order to verify the acoustic simulation results, hydrophone measurements were performed in deionized and degassed water for both the single focus and multifoci sonication patterns. The measurements were done with a needle hydrophone (75 μm diameter, Precision Acoustics, UK) attached to a 3D motion control system consisting of three linear M-ILS250PP stages (Newport, Irvine, CA), stepper driver NI-MID-7604, and motion controller PXI-7354 (National Instruments, Austin, TX). The signals were sampled using a 100 MHz high-speed digitizer PXI-5122 (National Instruments, Austin, TX).

For both sonication patterns, a plane perpendicular to the beam axis was acquired with resolution of 0.1 × 0.1 mm^2 and FOV of 12 × 12 mm^2. In the beam axis direction, the planes were positioned at the maximum pressure of the single focus measurement. Tone bursts of 40 cycles at center frequency of 1.45 MHz were used. Acoustic peak power was approximately 25 W. The acquired acoustic signals were filtered in Fourier space to remove the nonlinear (high frequency) components that are typically attenuated rapidly in tissue, but tend to accumulate in nonattenuating water. This improved the signal-to-noise ratio and ensured a fair comparison with simulations that utilized a linear propagation model. Measurements were performed in quasilinear conditions, i.e., the local distortion parameter was well below 0.5.[50]

II.D. *In vitro* and *in vivo* experiment setups

For the *in vitro* experiments, a tissue-mimicking gel-phantom was prepared from a mixture of agarose (2 wt. %, VWR International, Radnor, PA) and 0.5–10 μm silica particles (2 wt. %, Sigma-Aldrich, Schnelldorf, Germany) in deionized and degassed water as previously described.[42,51] This mixture was heated with constant stirring to prevent settling of silica, and then slowly cooled until gelled. The resulting gel phantom had an estimated ultrasound propagation speed of 1490 m/s, and an ultrasound attenuation of 0.65 dB/cm at 1.45 MHz. The phantom was positioned on the acoustic window of the HIFU tabletop and acoustically coupled using degassed, deionized water.

Animal-related procedures were approved and carried out under a National Institutes of Health animal care and use protocol. The Vx2 tumor preparation and animal setup was described by Ranjan *et al.*[52] Briefly, the superficial thigh muscle of a New Zealand White rabbit (n = 1, body weight = 2.8 kg) was inoculated with Vx2 tumor cells and allowed to grow to size (>1.5 cm in any dimension). Acoustic

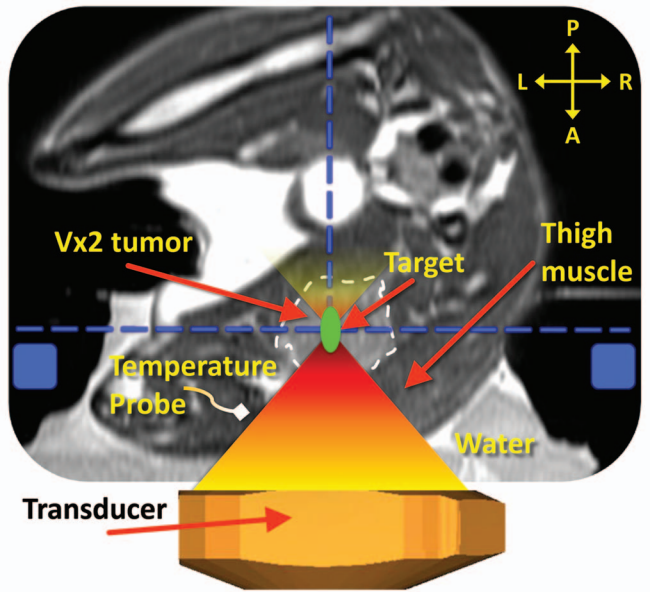

FIG. 1. Schematic of the experimental MR-HIFU hyperthermia setup. The axial imaging plane is shown, with the rabbit in right lateral decubitus position on top of the HIFU tabletop and the tumor-bearing right hind limb submerged in degassed water. Vx2 tumor is outlined with a white dashed line. Baseline reference temperature was obtained using a fiber optic temperature probe inserted in the thigh muscle near the tumor. The imaging slice positions for the thermometry sequence are outlined with a blue dashed line, and the location of the MR coil used for temperature mapping is shown as blue rectangles. A target region within the tumor is shown as a green circle. A, P, L, and R denote anterior, posterior, left, and right, respectively. Depictions of the MR coil, the transducer, and HIFU beam propagation are only illustrative and not to scale.

coupling was achieved by submerging the tumor-bearing thigh in a degassed water bath directly above the transducer (Fig. 1). A dedicated optical temperature probe (diameter = 0.56 mm, Luxtron 3100, LumaSense Technologies, Santa Clara, CA) was inserted in the thigh muscle near the tumor, and used as the baseline temperature for MR thermometry, which was updated prior to each sonication. At the end of the *in vivo* MR-HIFU experiment, the animal was immediately euthanized by intravenous injection of Beuthanasia III (dose = 0.2 ml/kg, Pentobarbital Sodium 390 mg/ml, and Phenytoin Sodium 50 mg/ml). Post-treatment, tissue samples were harvested for further analysis both from the treated tumor and muscle as well as from adjacent surrounding tissue.

II.E. MR-HIFU platform and MR imaging

A clinical integrated MR-HIFU platform (Sonalleve V1 1.5T MR-HIFU, Philips Medical Systems, Vantaa, Finland) was utilized both for sonications and MR guidance, using clinical software that was modified to suit small animal studies and to perform multifoci sonications. The system also included two coils: a MR-HIFU specific multielement MR receive coil used for treatment planning, and a standard two-element loop coil (SENSE Flex M, Philips Medical Systems, Best, The Netherlands) used for temperature mapping. A 256-element focusing phased-array transducer (12 cm radius of curvature, 13 cm aperture) was operated at 1.45 MHz for all sonications. For the single focus sonications, the *in situ* intensity (I_{spta}) (Ref. 53) at the focus for a 25 W sonication was estimated to be 400 W/cm^2 at a sonication depth of 15 mm in tissue assuming an attenuation coefficient of 0.5 dB cm^{-1} MHz^{-1}.[45]

MRI was used to plan the therapy as well as to monitor temperature rise with temperature sensitive imaging during therapy. Prior to therapy, proton density-weighted planning images were acquired as a 3D coronal stack and used for ultrasound exposure planning. Standard multiplane thermometry was performed during HIFU sonications using a dynamic fast field echo-echo planar imaging (FFE-EPI) sequence. Two image slices were acquired per dynamic scan repetition; one coronal and one sagittal slice automatically positioned perpendicularly and parallel to the HIFU beam axis with the slices intersecting at the center of the target region (Fig. 1). Identical imaging parameters were used for both slices: TR = 54 ms, TE = 30 ms, spatial resolution 1.4 × 1.4 mm^2, slice thickness = 7 mm, 7 k-space lines per excitation, flip angle = 19°, 121-binomial water-selective excitation, resulting in an acquisition time of 2.5 s per dynamic scan repetition. The same sequence was used for *in vitro* experiments, but with slightly different imaging parameters (TR = 44 ms, TE = 20 ms, slice thickness = 5 mm), with an acquisition time of 2.0 s per dynamic scan repetition. SNR-masked temperature maps (masked when temperature standard deviation > 3 °C) were calculated in real time from the resulting phase images using the PRFS (0.0094 ppm/°C) technique.[19] All voxels where $\Delta T > 2\,^{\circ}C$ were color encoded and overlaid on top of the grayscale magnitude images. The obtained temperature maps were corrected for baseline drift by subtracting the average apparent temperature change of the voxels within a freely defined reference region that was placed near but outside the heated region in the coronal slice. Additional details may be found in Refs. 42 and 39.

II.F. Mild hyperthermia feedback control

In this study, binary mild hyperthermia feedback as described by Partanen *et al.*[42] was used to control volumetric heating. The sonication time at each subtrajectory was determined by predefined temperature limits. Briefly, the sonication started at the innermost heat-up subtrajectory, and was moved from one heat-up subtrajectory to the next once the mean upper temperature limit was reached. After the outermost heat-up subtrajectory had been completed, sonication was paused. Once the mean temperature at any subtrajectory dropped below the lower mean temperature limit, the sonication was moved to that subtrajectory. Sonication was once again paused when the mean temperature in that subtrajectory reached the upper mean temperature limit. These heating and cooling cycles were repeated until the predefined sonication duration expired. Binary mild hyperthermia feedback control was achieved by setting the lower mean temperature limit to 40.5 °C and the upper mean temperature limit to 41.0 °C.

II.G. Sonication experiments

Sonication experiments were performed both *in vivo* and in a tissue-mimicking phantom. Before starting the therapy sonications, a low-power test-sonication (P_{ac} = 15 W, t = 10 s) was performed in the target volume in order to adjust and confirm the correct location of heating. In the *in vivo* study, the duration of each hyperthermia treatment was 5 min and the target region (also known as a treatment cell) was 8 mm in diameter. Both Vx2 tumor and normal muscle were targeted. Between sonications, a fixed cool down period (5 min) was employed to ensure return to baseline temperature. Sonications were performed at five different locations in each tumor and muscle tissue for both the single focus and multifoci sonication strategies (total of 20 sonications). In this implementation, the target region was defined only in the coronal slice. However, it is also important to characterize the heating shape in 3D. This is perhaps best described by the aspect ratio of heated region, i.e., the ratio of length in the beam path direction to diameter perpendicular to the beam path.

In the phantom experiments, the temperature limits remained the same, but sonication duration was 10 min and cool-down time between sonications was increased to 30 min primarily because there is no perfusion to actively cool the phantom. Both single focus and multifoci sonication experiments were performed with treatment cell sizes of 4, 8, 12, and 16 mm in diameter. Each experiment was repeated five times (total of 40 sonications).

In both animal and phantom experiments, a MR-compatible passive cavitation detector (integrated into the HIFU transducer) was used to detect possible cavitation during sonication.

TABLE II. Summary of the mild hyperthermia sonications performed *in vivo* and *in vitro*. All sonications were performed at a frequency of 1.45 MHz. Duration of 5 min was used for sonications *in vivo* and 10 min for sonications *in vitro*.

	Sonication type	Treatment cell size (mm)	Target tissue	Acoustic power (W)	Number of sonications	Focal depth from skin (mm)
Rabbit	Single focus	8.0	Tumor	25.0	5	30
Rabbit	Multifoci	8.0	Tumor	25.0	5	30
Rabbit	Single focus	8.0	Muscle	25.0	5	15
Rabbit	Multifoci	8.0	Muscle	25.0	5	15
Phantom	Single focus	4.0, 8.0, 12.0, 16.0	...	25.0	5, 5, 5, 5	40
Phantom	Multifoci	4.0, 8.0, 12.0, 16.0	...	25.0	5, 5, 5, 5	40

Table II summarizes the mild hyperthermia sonications performed in the phantom and in the animal. All heat-maintaining subtrajectories were sonicated at half the power used for the initial heat-up subtrajectories.

II.H. Hyperthermia treatment analysis and statistical analysis

Data were analyzed with MATLAB 7.0 (MathWorks, Natick, MA) and in-house developed software package for IDL 6.1 (ITT Visual Information Solutions, Boulder, CO). The mean temperature, lowest tenth percentile (T90), highest tenth percentile (T10), and SD in the target region were analyzed from the coronal slice to assess temperature accuracy and uniformity. Heated volume length, diameter, and their ratio were also quantified. Heated region diameter and length were calculated from coronal and sagittal slices, respectively, as mean distances with temperature $\geq 40.5\,^{\circ}\mathrm{C}$ (calculated from time-averaged data once $T > 39.5\,^{\circ}\mathrm{C}$). Furthermore, thermal dose accumulation in the target region was calculated according to the Sapareto-Dewey equation and reported using a unit of equivalent minutes at 43 °C (CEM_{43}).[54] Values are reported as mean ± standard deviation, unless stated otherwise.

All data fitting and statistical analyses were performed using GraphPad Prism (version 5.04 for Windows, San Diego, CA). One-way ANOVA was performed to compare the distributions of mean temperature, T_{10-90}, width of the heated volume over 40.5 °C, and the ratio of the length to the diameter of the heated volume. Pairwise comparisons with Tukey multiple comparison test were reported. Two-tailed p-values were obtained in all cases, with $p < 0.05$ considered significant.

III. RESULTS

III.A. Acoustic field simulations and thermal simulations

Simulated acoustic fields (pressure arbitrary units) for an 8 mm diameter (16 foci, phase increment of 180°) multifoci pattern as well as for a single focal point deflection (4 mm) are shown in Fig. 2. The total acoustic power was the same for both cases. All acoustic simulation results are provided in Table III. The maximum pressure is reduced by 70% with multifoci implementation as compared to single focus.

In silico temperature distribution at the end of 10 min sonications are shown in Fig. 3 for both single focus sweep and multifoci approaches, using an 8 mm diameter target region.

All thermal simulation results are provided in Table III. The multifoci implementation provided a more homogeneous heated region that was closer to the intended target diameter and also to the intended location in the beam axis direction. However, the heating energy efficiency is also reduced as the volume heated above 40.5 °C is significantly smaller even though a similar amount of energy is used for both the single focus (1890 J) and multifoci (1840 J) sonication approaches.

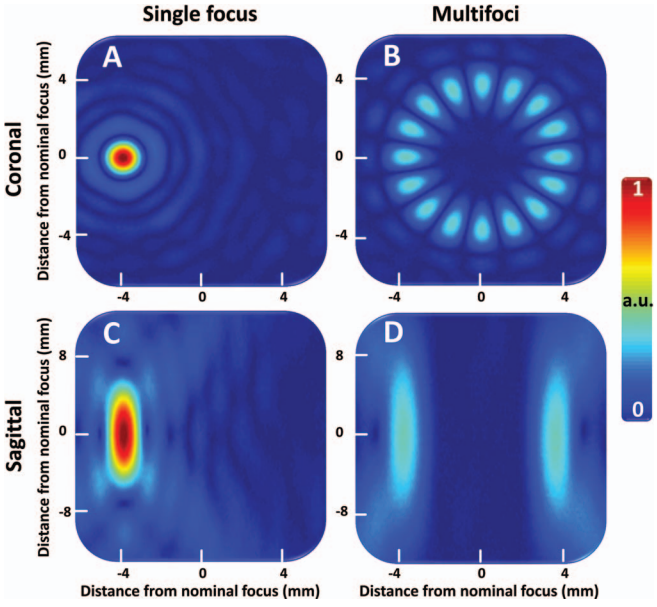

FIG. 2. (a) and (b) Simulated acoustic pressure field (focal plane) for a single focal point deflection 4 mm to the left in the image coordinates (a), as well as for a multifoci sonication with 16 simultaneous foci spaced evenly at a circle with 8 mm diameter (b). (c) and (d) are the sagittal image planes (beam path direction) corresponding to (a) and (b), respectively. Transducer sonicates from bottom to top in the sagittal images.

TABLE III. Summary of results for both single focus and multifoci sonications (8 mm target region).

Heating phase	Focus mode	No. of conc. foci	Mean T in mask (°C)	Peak T (°C)	T10 (°C)	T90 (°C)	T_{10-90} (°C)	Appl. power (W)	Max. intensity (W/cm^2)	Max. pressure (MPa)	CM of 40.5 °C vol. in beam path dir. (mm)	Vol. above 40.5 °C (mm^3)	40.5 °C vol. diam. (mm)	40.5 °C vol. length (mm)	40.5 °C vol. length to diam. ratio	Heating energy efficiency (mm^3/J)
4 mm subtrajectory heat-up, t = 60 s	Single focus	1	40.92	41.17	41.08	40.73	0.35	3.49	74.09	1.52	−2.35	113.68	4.48	10.2	2.28	0.54
	Multifoci	8	40.87	41.13	41.01	40.70	0.31	3.74	15.34	0.69	−1.34	108.12	4.36	7.2	1.65	0.48
8 mm subtrajectory heat-up, t = 180 s	Single focus	1	40.80	41.52	40.96	40.67	0.29	4.19	82.43	1.61	−6.97	827.61	8.8	16.5	1.88	1.65
	Multifoci	16	40.79	41.02	40.92	40.64	0.28	3.96	7.37	0.48	−3.78	565.75	7.96	11.25	1.41	1.19
8 mm subtrajectory maintenance, t = 600 s	Single focus	1	40.78	41.37	40.92	40.65	0.27	2.81	55.30	1.32	−7.14	932.01	9.12	16.8	1.84	0.79
	Multifoci	16	40.75	40.93	40.85	40.65	0.20	2.71	5.04	0.40	−4.45	666.40	8.4	11.7	1.39	0.59

Note: No. = number; conc. = concurrent; T = temperature; appl. = applied; max. = maximum; CM = center of mass; dir. = direction; vol. = volume; diam. = diameter.

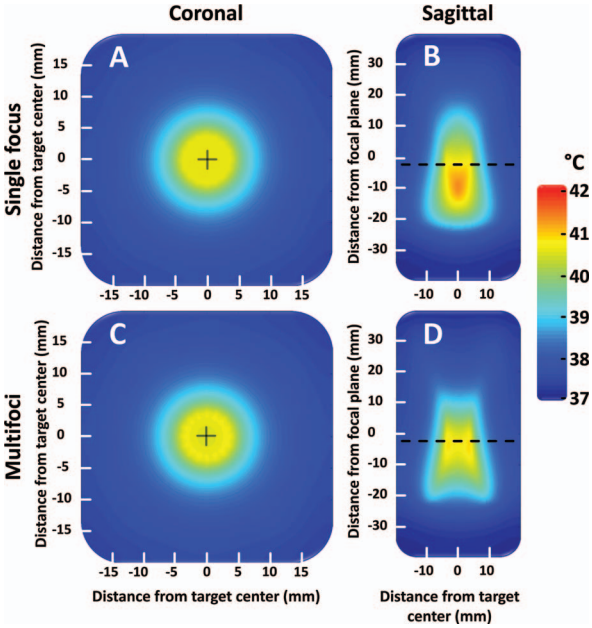

FIG. 3. (a) and (b) Simulated temperature distribution obtained by using a conventional 8 mm sonication trajectory where a single focal point is swept temporally across the 16 focal points included in the trajectory. The sweeping is very rapid (50 ms per sonication location) and in effect equals temporal averaging. (a) Coronal after 600 s, (b) sagittal after 600 s. (c) and (d) Simulated temperature distribution obtained by using the multifoci pattern with 16 concurrent foci as shown in Fig. 2. (c) Coronal after 600 s, (d) sagittal after 600 s. Transducer sonicates from bottom to top in the sagittal images.

III.B. Hydrophone measurements

Hydrophone measurements for the 8 mm multifoci pattern (16 foci, phase increments of 180°) as well as for a single focal point deflection are shown in Fig. 4. In addition to

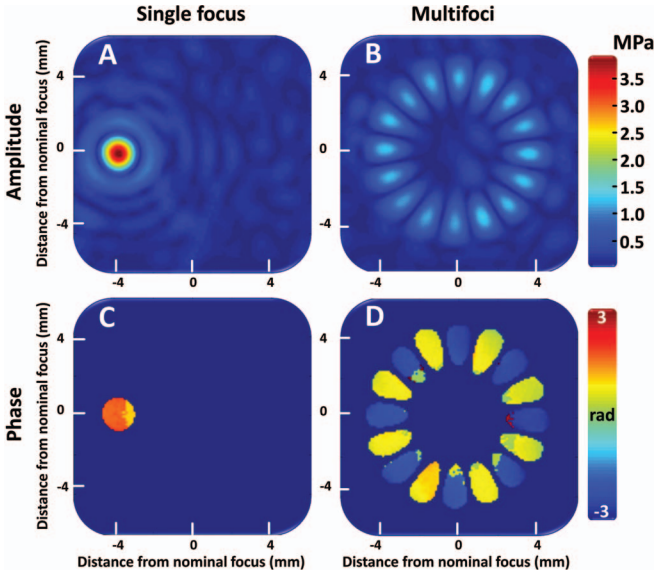

FIG. 4. Acoustic pressure field distributions obtained using a needle hydrophone. (a) Single focal point deflection 4 mm to the left in the image coordinates. (b) Multifoci sonication with 16 simultaneous foci spaced evenly at a circle with 8 mm diameter. (c) and (d) are the phase maps corresponding to pressure maps (a) and (b), respectively.

TABLE IV. Summary of *in vitro* sonication results. Target mean temperature range was 40.5–41 °C. All values are mean ± SD of five sonications. Heated region diameter and length to diameter ratio were calculated from time-averaged data.

Treatment cell size (mm)	Sonication type	Mean (°C)	SD (°C)	T10 (°C)	T90 (°C)	Diameter of area ≥ 40.5 °C (mm)	Volume ≥ 40.5 °C length to diameter ratio
4.0	Single focus	40.90 ± 0.06	0.68 ± 0.08	41.75 ± 0.12	40.13 ± 0.04	4.4 ± 0.2	2.9 ± 0.3
8.0	Single focus	40.94 ± 0.05	0.64 ± 0.06	41.67 ± 0.11	40.12 ± 0.11	8.6 ± 0.4	2.2 ± 0.2
12.0	Single focus	40.97 ± 0.08	0.71 ± 0.07	41.8 ± 0.2	40.14 ± 0.03	11.2 ± 0.3	2.4 ± 0.2
16.0	Single focus	41.24 ± 0.08	0.87 ± 0.04	42.32 ± 0.09	40.21 ± 0.08	15.0 ± 0.7	1.9 ± 0.1
4.0	Multifoci	40.76 ± 0.05	0.60 ± 0.03	41.51 ± 0.11	40.06 ± 0.05	3.96 ± 0.11	2.0 ± 0.4
8.0	Multifoci	40.74 ± 0.04	0.56 ± 0.02	41.45 ± 0.13	40.14 ± 0.07	8.0 ± 0.2	1.7 ± 0.2
12.0	Multifoci	40.73 ± 0.04	0.68 ± 0.08	41.60 ± 0.15	40.07 ± 0.09	11.4 ± 0.3	1.4 ± 0.2
16.0	Multifoci	40.74 ± 0.04	0.66 ± 0.05	41.59 ± 0.12	39.94 ± 0.06	15.2 ± 0.2	1.26 ± 0.11

magnitude (pressure) maps, the phase maps are shown to illustrate the 180° phase difference between adjacent foci. Splitting the focus was successful for the multifoci approach, resulting in the prescribed number of discrete foci. Although the comparison of the measured pressure maps to the simulations was qualitative, Figs. 2(b) and 4(b) demonstrate a close similarity.

The maximum focal pressures were 3.7 and 1.2 MPa for the single focus and multifoci measurement, respectively. For the multifoci pattern, the pressure dropped by approximately 68% from that of the single focus pattern, which is a similar reduction as seen in the simulations (see Table III).

III.C. *In vitro* MR-HIFU mild hyperthermia

All *in vitro* results are provided in Table IV. Mean temperatures in the treatment cell corresponded well with the target temperature range (target T = 40.5–41 °C) for both sonication approaches. The temperature in the treatment cell was slightly but significantly ($p < 0.05$, Tukey) higher in single focus sonications (range = 40.81–41.32 °C) than in multifoci sonications (range = 40.69–40.82 °C) for all treatment cell sizes. The temperature uniformity, indicated by a smaller $T_{10–90}$, was significantly better for the multifoci approach in the 8 and 16 mm treatment cells ($p < 0.05$, Tukey). Diameters of the heated volumes (≥ 40.5 °C) were similar for both sonication strategies in large treatment cells (12 and 16 mm) but were significantly larger for the single focus approach in the smaller treatment cells (4 and 8 mm cells, $p < 0.05$, Tukey), see Table IV. The ratio of the length to diameter of the heated region was significantly smaller for the multifoci approach (range = 1.26–2.0) than for the single focus heating (range = 1.9–2.9) for all cell sizes ($p < 0.05$, Tukey). This indicates that the heating was better confined in the beam path direction for the multifoci approach. Cavitation was not observed during any of the *in vitro* sonications.

III.D. Treatment planning and temperature imaging

MRI was used for treatment planning as well as temperature imaging, as shown in Fig. 5. Quality and contrast in planning images were sufficient to identify the tumor (hyperintense) from the surrounding normal tissue and then plan the treatment cell locations (Fig. 5). Location of the hyperthermic region attained during treatment corresponded well with target location. Although spatial targeting accuracy was not rigorously analyzed, it appeared similar to what was previously reported using the same MR-HIFU device and temperature monitoring method.[42] Temperature maps *in vivo* had a mean noise level of 0.3 ± 0.1 °C.

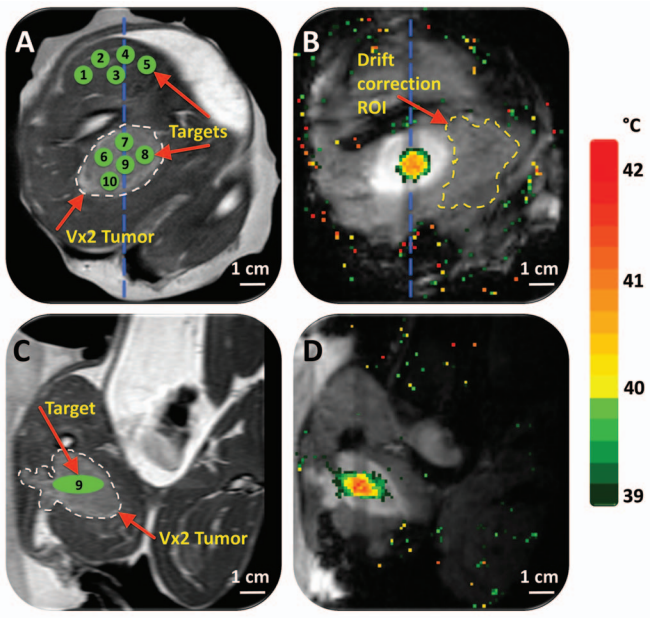

FIG. 5. Planning and temperature mapping for mild hyperthermia using multifoci sonication approach: (a) Vx2 tumor (hyperintense) was clearly identified (white dashed line) on the proton density-weighted planning images and target regions both within the tumor and normal muscle were chosen (green circles). (b) Temperature maps (color scale) overlaid on dynamic magnitude images (grayscale) during a mild hyperthermia treatment with an 8 mm treatment cell, showing typical temperature distribution after 3 min of heating. Temperature monitoring and control was achieved in the selected target region with a FFE-EPI imaging sequence, utilizing the PRFS method for temperature mapping, and by using mild hyperthermia binary feedback control algorithm. The ROI used for magnetic drift correction is outlined with a yellow dashed line. (c) and (d) are the sagittal image planes corresponding to (a) and (b), respectively, the location of which is outlined with a blue dashed line in (a) and (b). In (d), far-field temperature mapping artifacts arising from bowel movement have been suppressed in postprocessing.

TABLE V. Summary of *in vivo* sonication results. Treatment cell size was 8 mm and target mean temperature range was 40.5–41 °C. All values are mean ± SD of five sonications. Heated region diameter and length to diameter ratio were calculated from time-averaged data.

Sonication type	Target tissue	Mean (°C)	SD (°C)	T10 (°C)	T90 (°C)	Diameter of area ≥ 40.5 °C (mm)	Volume ≥ 40.5 °C length to diameter ratio	Mean thermal dose (CEM_{43})
Single focus	Tumor	40.82 ± 0.12	0.65 ± 0.05	41.60 ± 0.09	39.98 ± 0.20	8.1 ± 0.2	2.0 ± 0.5	0.34 ± 0.04
Multifoci	Tumor	40.70 ± 0.09	0.64 ± 0.04	41.4 ± 0.2	39.96 ± 0.14	8.0 ± 0.2	1.3 ± 0.2	0.28 ± 0.04
Single focus	Muscle	40.99 ± 0.10	0.74 ± 0.14	41.8± 0.2	40.1 ± 0.2	8.68 ± 0.30	1.95 ± 0.25	0.5 ± 0.2
Multifoci	Muscle	40.69 ± 0.07	0.69 ± 0.06	41.51 ± 0.14	39.94 ± 0.10	8.55 ± 0.12	1.52 ± 0.27	0.35 ± 0.06

III.E. *In vivo* MR-HIFU mild hyperthermia

All *in vivo* results are reported in Table V. For both sonication approaches, *in vivo* volumetric sonications resulted in roughly ellipsoid-shaped temperature elevations with the major axis in the direction of the HIFU beam propagation and a circular-symmetric cross section in the coronal plane (Fig. 5), in good concordance with simulations, phantom experiments, and previously reported results.[39,42,43] Mean temperature in the treatment cell rapidly reached the upper temperature limit (heating rate 0.13–0.21 °C/s, typically faster for the single focus sweep method) as shown in Fig. 6. The faster heat-up for the single focus sweep also resulted in greater initial temperature overshoot (see Fig. 6). During the temperature maintenance phase, temperature stability was similar for both sonication methods. Upon completion of the sonication, temperature in the treatment cell returned to baseline levels over approximately 5 min. Agreement of temperature before and after sonication suggests that the magnetic drift correction was adequately applied. Cavitation was not observed by the integrated passive cavitation detector during any of the *in vivo* sonications.

In vivo sonications using 8 mm treatment cells in muscle and in tumor resulted in roughly the same circular area of hyperthermia (≥40.5 °C, diameter not significantly different) in the coronal plane for both sonication approaches, as shown in Table V and in Figs. 7 and 8, corresponding well with the nominal cell size. However, in the sagittal plane (beam axis direction) the multifoci sonications resulted in significantly shorter heated volumes in tumor ($p < 0.05$, Tukey) as shown in Fig. 8, and slightly but not significantly shorter heated volumes in muscle (see Table V). Although the difference between T10 and T90 was lower for multifoci (range = 1.32–1.73 °C) than for single focus (range = 1.41–2.27 °C), overall comparison showed no significant difference for this metric (ANOVA, $p = 0.1370$). Importantly, the differences between T10 and T90 were low with both approaches, indicating good temperature control within the treatment volume. Mean temperatures over the sonication duration in the treatment cell were within the target temperature range (target T = 40.5–41 °C) for both sonication approaches, and were slightly but significantly lower for the multifoci sonications in muscle ($p < 0.001$, Tukey), but not in tumor.

Tissue damage was not rigorously evaluated, but no mechanical or thermal damage was evident in the dissected tissue, consistent with the lack of cavitation and with the low thermal dose delivered per sonication (mean $CEM_{43} \leq 0.53$, see Table V).

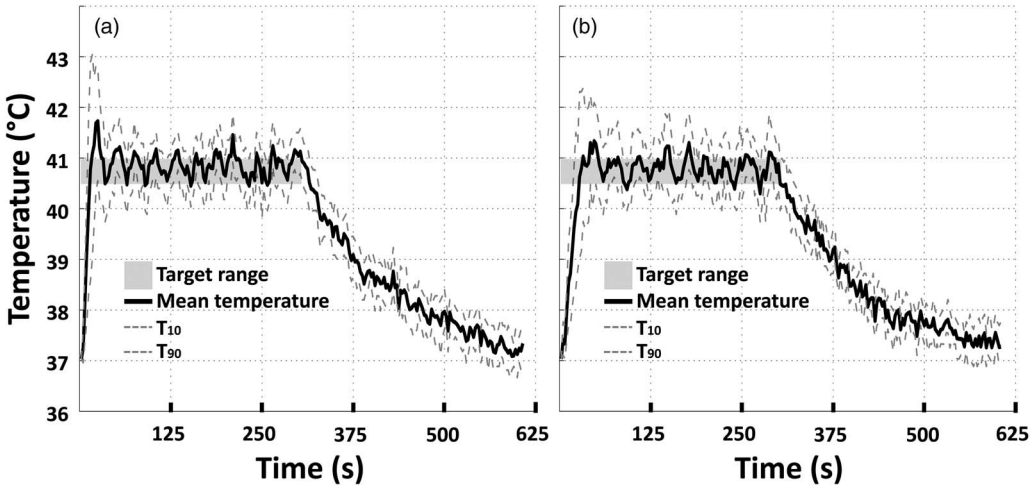

FIG. 6. (a) Representative examples of mean (solid), T10, and T90 (dashed) temperatures within an 8 mm treatment cell over a 5 min sonication *in vivo* using the single focus sweep approach. Target temperature range is indicated as a gray box. (b) Representative examples of mean (solid), T10, and T90 (dashed) temperatures within an 8 mm treatment cell over a 5 min sonication in Vx2 tumor using the multifoci approach. Target temperature range is indicated as a gray box.

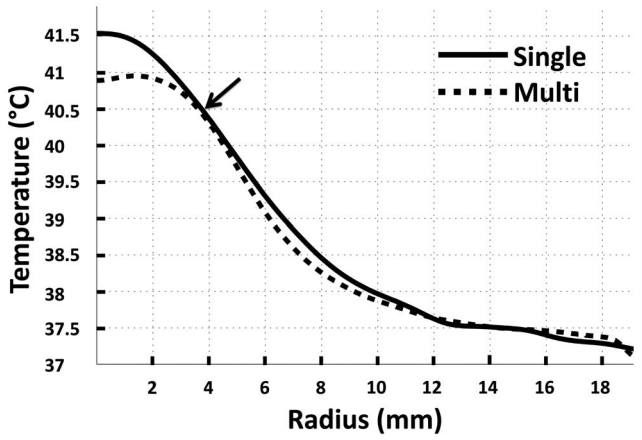

FIG. 7. Representative examples of time-averaged mean temperature radial line profiles centered on the 8 mm treatment cell in Vx2 tumor for both single focus and multifoci sonication approaches. The lower target temperature limit (40.5 °C) and the corresponding heated volume radii for both single focus (3.9 mm) and multifoci (3.8 mm) sonications are indicated with an arrow.

IV. DISCUSSION

Monitoring and control of acoustic bioeffects of HIFU is paramount to realizing a safe and effective clinical treatment, requiring a balance of therapeutic goals and potential risks. Leveraging acoustic bioeffects related to high pressure such as acoustic cavitation and acoustic radiation force may improve the therapy of multiple diseases including cancer and thromboembolic diseases.[55,56] However, precisely controlling these bioeffects in a diverse patient population may pose a significant challenge for clinical translation, and additional technological advances may therefore be necessary to control or monitor these bioeffects in a clinical setting. Our goal was to provide mild hyperthermia in a safe, controlled, and efficacious manner, while aiming to avoid bioeffects related to high acoustic pressures. This goal was realized on a clinical MR-HIFU platform by implementing a well-known approach to generate multiple foci by manipulating the amplitude and phase of the individual transducer element driving signals.[36,37] Previously, multiple simultaneous foci have been used for hyperthermia induced local drug delivery to enlarge the heated region as compared to a single static focus.[57]

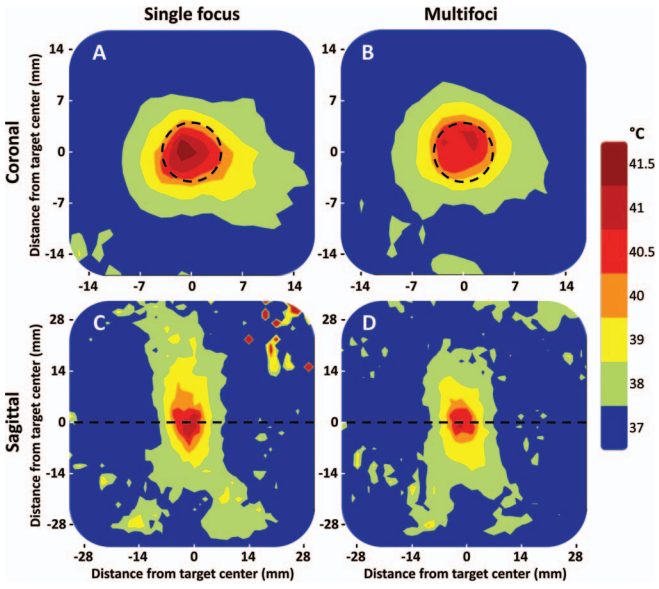

FIG. 8. (a) and (c) Representative examples of time-averaged spatial temperature distributions for the 8 mm treatment cell in Vx2 tumor for single focus sweep sonication approach (coronal and sagittal planes). (b) and (d) Representative example of time-averaged spatial temperature distributions for the 8 mm treatment cell in Vx2 tumor for multifoci sonication approach (coronal and sagittal planes). The treatment cell is outlined by the black dashed circles in the coronal images (a) and (b), whereas the black dashed lines in the sagittal images (c) and (d) depict the location of the coronal slices. In the sagittal images (c) and (d), the transducer sonicates from bottom to top.

The current single focus sweep approach for MR-HIFU mediated mild hyperthermia, using rapid and sequential electronic steering of the ultrasound beam,[42,52,58] is a feasible and attractive heating strategy due to the efficient localized heating. However, this approach might also suffer from instantaneous, high, and localized acoustic pressures and intensities, leading to unfavorable mechanical effects and nonuniform and thus less controlled or less predictable heating in tissue. As an example of unwanted mechanical effects, recent preclinical studies on HIFU have shown an enhanced metastatic burden at high levels of acoustic pressure (5 MPa) and in the presence of shock waves and acoustic cavitation.[59–61]

Compared to single focus sweep sonications, the multifoci mild hyperthermia approach provided reduced acoustic pressures in the focal region (see Table III), according to acoustic simulations and hydrophone measurements (1.2 MPa vs 3.7 MPa for multifoci and single focus, respectively). While the mechanical index (MI) has been used in diagnostic ultrasound exposures to assess the probability of deleterious mechanical tissue damage, a general consensus on a similar metric for appraising mechanical damage due to HIFU exposures has not been established. Nonetheless, the pressures achieved in this work (2.6 MPa/MHz) are clearly below a HIFU threshold suggested by Hynynen[62] for onset of acoustic cavitation (5.3 MPa/MHz). The multifoci sonication approach may find use in applications where mechanical tissue damage is not warranted (e.g., drug delivery and radiation sensitization). Deep-seated tumors or targets with high perfusion may require greater acoustic power, leading to higher peak pressures. Multifoci sonications may be used to reduce peak acoustic pressures and intensities to safe levels, eliminating unwanted cavitation and/or mechanical tissue damage.

Combined with a binary feedback algorithm, the multifoci heating method provided robust temperature control resulting in better temperature uniformity in the target region in both simulations and experiments, although the difference was not statistically significant in vivo (mean $T_{10-90} = 1.41$ vs 1.62 °C for multifoci vs single focus in tumor, respectively). The temperature elevations in the HIFU beam-path direction were also consistently more spatially confined in the multifoci approach (mean heated volume length in beam path direction to diameter perpendicular to the beam path ratio $= 1.3 \pm 0.2$ vs 2.0 ± 0.5 in tumor). A higher ratio may allow heating of larger volumes with less energy resulting in greater heating efficiency, although this is not of substantial concern for mild hyperthermia where thermal damage to skin or near field is unlikely due to the low target temperatures.

However, a length to diameter ratio closer to 1 may in turn give more flexibility in prescribing target regions with diverse geometries, especially when confined in the beam axis. Additionally, the combined use of multifoci and single focus sweep sonications may better conform to specific geometries.

For the aforementioned reasons, this multifoci sonication strategy is an attractive candidate for initial translation of MR-HIFU mediated mild hyperthermia to a clinical setting due to the lower probability of unwanted and/or unpredictable mechanical or thermal effects, and due to the shorter heated regions, which could translate into confined heating and more controlled conformability. Furthermore, regulatory implications may also be favorable for lower acoustic pressures.

IV.A. Generation of sonication patterns

The number of focal points that can be heated simultaneously depends on the intended spatial separation as well as focal spot size, which again is determined by ultrasound wavelength and transducer geometry/design. Suboptimal separation of focal points increases acoustic intensity in the target region, negating the benefits of using the multifoci approach. Thus, in all experiments and simulations, the control points were separated by at least the diameter of one focal spot.

Phase at the control points was chosen in order to limit unwanted off-target heating. For example, if the phase is identical at all control points, coherences along the beam axis result in pronounced side lobes above and below the target volume. This effect can be mitigated by alternating phase between neighboring control points.[37] However, the phase increment between control points must be chosen carefully, as its choice has an effect on the pressure field. The chosen phase increment of 180° between neighboring points resulted in significantly reduced length of the heated volume, thereby preventing undesired temperature elevations in the HIFU beam-path direction outside the target region (see Table III and Figs. 3 and 8).

Despite their benefits, multifoci patterns might be less robust to imperfections in element amplitude and phase control caused by, e.g., deviation in the shape of the transducer from expected or heterogeneities in the acoustic path of individual elements. However, simulations suggest that with the expected amplitude and phase variations for this MR-HIFU setup, the multifoci patterns are not significantly affected (data not shown). This was also confirmed in hydrophone measurements where the prescribed multifoci spot generation was successfully obtained (Fig. 4). Furthermore, amplitude and phase variations due to heterogeneities in the acoustic path did not appear to alter the performance of the multifoci approach *in vivo* at a target depth of 15–30 mm. If observed at greater depths in future studies, the aforementioned problems could be addressed by reducing the number of concurrent foci.

IV.B. Hydrophone measurements

The measured multifoci patterns match very well with simulation results. The use of 8 mm diameter 16-foci multifoci pattern resulted in a maximum acoustic pressure reduced to 33% of the maximum pressure measured using single focus deflection, similar to what was seen in simulations. The consistency of simulation results with hydrophone measurements aids in validating the model and allows for additional future *in silico* optimization for more custom or patient-specific treatments.

IV.C. Temperature accuracy, temporal control, and homogeneity of heating

Results of the *in vivo* 8 mm treatment cell sonications using the multifoci approach are consistent with simulation and phantom experiment results, suggesting that temperature homogeneity may be improved through the use of this multifoci sonication strategy. Furthermore, the multifoci sonication approach may offer benefits in terms of shorter heated volumes in the beam axis direction, limiting thermal exposure in the direct near- and far-field.

Both heating approaches achieved *in vivo* mean temperatures that were prescribed by the target temperature range (40.5–41 °C). For the multifoci approach, mean temperature was lower with a more flat profile in the prescribed region (Fig. 7). Less overshoot was apparent for the multifoci approach during heat-up (Fig. 6), but adjusting the power used during heat-up for each strategy may further ameliorate this overshoot.

IV.D. Future directions

Traditional sonication trajectories that involve rapid HIFU steering through single focus points, as used in MR-HIFU volumetric thermal ablations,[40,63] tend to exhibit elongated heated volume shape in the beam axis direction. This approach with high heating energy efficiency may benefit ablation of large volumes. However, the heating outside the target plane with single focus sonications may limit application of MR-HIFU heating in small or shallow targets, or in close proximity to critical structures that must not be heated. The multifoci approach can produce more confined heating in the beam-axis direction by reducing the acoustic intensities at the spatial overlap that exists toward the near field. Thus, although the heating energy efficiency is lower, the multifoci approach may also have some use in HIFU thermal ablation.

Whether for ablation or for mild hyperthermia, the agreement between *in silico* modeling and *in vivo* heating suggests that such a modeling approach could be used to design patient- or application-specific multifoci patterns to assist in treatment planning. This modeling step may be necessary when high perfusion is likely to impact the spatial distribution of heat, or near critical structures where off-target heating may not be tolerated.

Volumetric multifoci patterns may also be beneficial in applications where mechanical effects need to be applied simultaneously to a large area or volume, such as in enhancement of drug delivery.[64] In this scenario, low duty-cycle pulsed sonications could be used to avoid excessive heating of the target, and power could be adjusted to compensate for the reduction in pressure with the multifoci approach.

Herein, we report on the initial evaluation of a multifoci sonication approach with small target volumes and short heating durations that is useful for development and characterization but very different than a prospective clinical implementation. For example, this approach may benefit large volume MR-HIFU mild hyperthermia methods that use a combination of mechanical movement of the transducer and electronic beam steering to heat large, more clinically relevant target volumes. These methods are currently under development. If incorporated into such a large-volume heating approach, multifoci sonications have the potential to decrease peak acoustic pressures, improve temperature uniformity, and limit off-target near-field heating.

V. CONCLUSION

This work demonstrates the potential benefits of a multifoci sonication approach combined with a binary feedback algorithm for mild hyperthermia on a clinical MR-HIFU platform. The implementation allowed for noninvasive, spatially accurate, precise, and homogeneous heating within the targeted regions in a tissue-mimicking phantom, in normal rabbit muscle, and in a Vx2 tumor. According to both simulations and hydrophone measurements, the multifoci approach produced lower acoustic pressures and intensities in comparison to the single focus sweep sonication method, thus potentially limiting unwanted mechanical effects that are of particular concern in mild hyperthermia. This multifoci heating strategy also provided more confined heated volume shape and improved temperature uniformity compared to the single focus approach, but at the cost of a reduced heating energy efficiency. Clinical oncology applications that require accurate and precise spatiotemporal control over heating (such as chemotherapeutic delivery and radiosensitization) may benefit from the improved safety and heating control offered by multifoci MR-HIFU mild hyperthermia.

ACKNOWLEDGMENTS

The authors thank Dr. Caitlin Burke, Dr. Ashish Ranjan, Dr. Carmen Gacchina, and David Woods for their support with animal studies. This research was supported by the Center for Interventional Oncology and Intramural Research Program of the National Institutes of Health (NIH), and through a Cooperative Research and Development Agreement (CRADA) with Philips Healthcare. Ari Partanen, Matti Tillander, and Dr. Max Köhler are paid employees of Philips Healthcare. The mention of commercial products, their source, or their use in connection with material reported herein is not to be construed as either an actual or implied endorsement of such products by the National Institutes of Health.

[a]Author to whom correspondence should be addressed. Electronic mail: max.kohler@philips.com

[1]B. J. Wood, J. R. Ramkaransingh, T. Fojo, M. M. Walther, and S. K. Libutti, "Percutaneous tumor ablation with radiofrequency," Cancer **94**, 443–451 (2002).

[2]B. L. Viglianti, P. Stauffer, E. Repasky, E. Jones, Z. Vujaskovic, and M. W. Dewhirst, "Hyperthermia," in *Holland-Frei Cancer Medicine*, edited by W. K. Hong *et al.* (People's Medical Publishing House, Shelton, CT, 2010), pp. 528–540.

[3]R. D. Issels, L. H. Lindner, J. Verweij, P. Wust, P. Reichardt, B. C. Schem, S. Abdel-Rahman, S. Daugaard, C. Salat, C. M. Wendtner, Z. Vujaskovic, R. Wessalowski, K. W. Jauch, H. R. Durr, F. Ploner, A. Baur-Melnyk, U. Mansmann, W. Hiddemann, J. Y. Blay, and P. Hohenberger, "Neo-adjuvant chemotherapy alone or with regional hyperthermia for localised high-risk soft-tissue sarcoma: A randomised phase 3 multicentre study," Lancet Oncol. **11**, 561–570 (2010).

[4]J. van der Zee, "Heating the patient: A promising approach?," Ann. Oncol. **13**, 1173–1184 (2002).

[5]M. H. Falk and R. D. Issels, "Hyperthermia in oncology," Int. J. Hyperthermia **17**, 1–18 (2001).

[6]P. Wust, B. Hildebrandt, G. Sreenivasa, B. Rau, J. Gellermann, H. Riess, R. Felix, and P. M. Schlag, "Hyperthermia in combined treatment of cancer," Lancet Oncol. **3**, 487–497 (2002).

[7]P. M. Krawczyk, B. Eppink, J. Essers, J. Stap, H. Rodermond, H. Odijk, A. Zelensky, C. van Bree, L. J. Stalpers, M. R. Buist, T. Soullie, J. Rens, H. J. Verhagen, M. J. O'Connor, N. A. Franken, T. L. Ten Hagen, R. Kanaar, and J. A. Aten, "Mild hyperthermia inhibits homologous recombination, induces BRCA2 degradation, and sensitizes cancer cells to poly (ADP-ribose) polymerase-1 inhibition," Proc. Natl. Acad. Sci. U.S.A. **108**, 9851–9856 (2011).

[8]J. J. Skitzki, E. A. Repasky, and S. S. Evans, "Hyperthermia as an immunotherapy strategy for cancer," Curr. Opin. Invest. Drugs **10**, 550–558 (2009).

[9]M. D. Hurwitz, "Today's thermal therapy: Not your father's hyperthermia: Challenges and opportunities in application of hyperthermia for the 21st century cancer patient," Am. J. Clin. Oncol. **33**, 96–100 (2010).

[10]L. Wu, R. J. McGough, O. A. Arabe, and T. V. Samulski, "An RF phased array applicator designed for hyperthermia breast cancer treatments," Phys. Med. Biol. **51**, 1–20 (2006).

[11]M. Weihrauch, P. Wust, M. Weiser, J. Nadobny, S. Eisenhardt, V. Budach, and J. Gellermann, "Adaptation of antenna profiles for control of MR guided hyperthermia (HT) in a hybrid MR-HT system," Med. Phys. **34**, 4717–4725 (2007).

[12]J. E. Johnson, D. G. Neuman, P. F. Maccarini, T. Juang, P. R. Stauffer, and P. Turner, "Evaluation of a dual-arm Archimedean spiral array for microwave hyperthermia," Int. J. Hyperthermia **22**, 475–490 (2006).

[13]T. Juang, P. R. Stauffer, D. G. Neuman, and J. L. Schlorff, "Multilayer conformal applicator for microwave heating and brachytherapy treatment of superficial tissue disease," Int. J. Hyperthermia **22**, 527–544 (2006).

[14]D. R. Boreham, H. C. Gasmann, and R. E. Mitchel, "Water bath hyperthermia is a simple therapy for psoriasis and also stimulates skin tanning in response to sunlight," Int. J. Hyperthermia **11**, 745–754 (1995).

[15]R. J. McNichols, M. Kangasniemi, A. Gowda, J. A. Bankson, R. E. Price, and J. D. Hazle, "Technical developments for cerebral thermal treatment: water-cooled diffusing laser fibre tips and temperature-sensitive MRI using intersecting image planes," Int. J. Hyperthermia **20**, 45–56 (2004).

[16]M. Kangasniemi, R. J. McNichols, J. A. Bankson, A. Gowda, R. E. Price, and J. D. Hazle, "Thermal therapy of canine cerebral tumors using a 980 nm diode laser with MR temperature-sensitive imaging feedback," Lasers Surg. Med. **35**, 41–50 (2004).

[17]T. O. Tasci, I. Vargel, A. Arat, E. Guzel, P. Korkusuz, and E. Atalar, "Focused RF hyperthermia using magnetic fluids," Med. Phys. **36**, 1906–1912 (2009).

[18]A. Jordan, P. Wust, H. Fahling, W. John, A. Hinz, and R. Felix, "Inductive heating of ferrimagnetic particles and magnetic fluids: physical evaluation of their potential for hyperthermia. 1993," Int. J. Hyperthermia **25**, 499–511 (2009).

[19]Y. Ishihara, A. Calderon, H. Watanabe, K. Okamoto, Y. Suzuki, and K. Kuroda, "A precise and fast temperature mapping using water proton chemical shift," Magn. Reson. Med. **34**, 814–823 (1995).

[20]B. D. de Senneville, B. Quesson, and C. T. Moonen, "Magnetic resonance temperature imaging," Int. J. Hyperthermia **21**, 515–531 (2005).

[21]K. Kuroda, A. H. Chung, K. Hynynen, and F. A. Jolesz, "Calibration of water proton chemical shift with temperature for noninvasive temperature imaging during focused ultrasound surgery," J. Magn. Reson. Imaging **8**, 175–181 (1998).

[22]W. J. Fry, V. J. Wulff, D. Tucker, and F. J. Fry, "Physical factors involved in ultrasonically induced changes in living systems: I. Identification of non-temperature effects," J. Acoust. Soc. Am. **22**, 867–876 (1950).
[23]W. D. O'Brien, Jr., "Ultrasound-biophysics mechanisms," Prog. Biophys. Mol. Biol. **93**, 212–255 (2007).
[24]M. Bailey, V. Khokhlova, O. Sapozhnikov, S. Kargl, and L. Crum, "Physical mechanisms of the therapeutic effect of ultrasound (a review)," Acoust. Phys. **49**, 369–388 (2003).
[25]D. Melodelima, J. Y. Chapelon, Y. Theillere, and D. Cathignol, "Combination of thermal and cavitation effects to generate deep lesions with an endocavitary applicator using a plane transducer: ex vivo studies," Ultrasound Med. Biol. **30**, 103–111 (2004).
[26]S. D. Sokka, R. King, and K. Hynynen, "MRI-guided gas bubble enhanced ultrasound heating in *in vivo* rabbit thigh," Phys. Med. Biol. **48**, 223–241 (2003).
[27]A. Yudina, M. de Smet, M. Lepetit-Coiffe, S. Langereis, L. Van Ruijssevelt, P. Smirnov, V. Bouchaud, P. Voisin, H. Grull, and C. T. Moonen, "Ultrasound-mediated intracellular drug delivery using microbubbles and temperature-sensitive liposomes," J. Controlled Release **155**, 442–448 (2011).
[28]V. Frenkel, J. Oberoi, M. J. Stone, M. Park, C. Deng, B. J. Wood, Z. Neeman, M. Horne III, and K. C. Li, "Pulsed high-intensity focused ultrasound enhances thrombolysis in an *in vitro* model," Radiology **239**, 86–93 (2006).
[29]C. K. Holland and R. E. Apfel, "Thresholds for transient cavitation produced by pulsed ultrasound in a controlled nuclei environment," J. Acoust. Soc. Am. **88**, 2059–2069 (1990).
[30]M. S. Canney, M. R. Bailey, L. A. Crum, V. A. Khokhlova, and O. A. Sapozhnikov, "Acoustic characterization of high intensity focused ultrasound fields: A combined measurement and modeling approach," J. Acoust. Soc. Am. **124**, 2406–2420 (2008).
[31]D. Dalecki, E. L. Carstensen, K. J. Parker, and D. R. Bacon, "Absorption of finite amplitude focused ultrasound," J. Acoust. Soc. Am. **89**, 2435–2447 (1991).
[32]K. Hynynen, "Demonstration of enhanced temperature elevation due to nonlinear propagation of focussed ultrasound in dog's thigh *in vivo*," Ultrasound Med. Biol. **13**, 85–91 (1987).
[33]E. Filonenko and V. Khokhlova, "Effect of acoustic nonlinearity on heating of biological tissue by high-intensity focused ultrasound," Acoust. Phys. **47**, 468–475 (2001).
[34]M. S. Canney, V. A. Khokhlova, O. V. Bessonova, M. R. Bailey, and L. A. Crum, "Shock-induced heating and millisecond boiling in gels and tissue due to high intensity focused ultrasound," Ultrasound Med. Biol. **36**, 250–267 (2010).
[35]D. R. Daum and K. Hynynen, "Thermal dose optimization via temporal switching in ultrasound surgery," IEEE Trans. Ultrason. Ferroelectr. Freq. Control **45**, 208–215 (1998).
[36]E. S. Ebbini and C. A. Cain, "Multiple-focus ultrasound phased-array pattern synthesis: Optimal driving-signal distributions for hyperthermia," IEEE Trans. Ultrason. Ferroelectr. Freq. Control **36**, 540–548 (1989).
[37]X. Fan and K. Hynynen, "Control of the necrosed tissue volume during noninvasive ultrasound surgery using a 16-element phased array," Med. Phys. **22**, 297–306 (1995).
[38]H. L. Liu, W. L. Lin, and Y. Y. Chen, "A fast and conformal heating scheme for producing large thermal lesions using a 2D ultrasound phased array," Int. J. Hyperthermia **23**, 69–82 (2007).
[39]M. O. Köhler, C. Mougenot, B. Quesson, J. Enholm, B. Le Bail, C. Laurent, C. T. Moonen, and G. J. Ehnholm, "Volumetric HIFU ablation under 3D guidance of rapid MRI thermometry," Med. Phys. **36**, 3521–3535 (2009).
[40]Y. S. Kim, B. Keserci, A. Partanen, H. Rhim, H. K. Lim, M. J. Park, and M. O. Köhler, "Volumetric MR-HIFU ablation of uterine fibroids: Role of treatment cell size in the improvement of energy efficiency," Eur. J. Radiol. **81**(11), 3652–3659 (2012).
[41]C. Mougenot, M. O. Köhler, J. Enholm, B. Quesson, and C. Moonen, "Quantification of near-field heating during volumetric MR-HIFU ablation," Med. Phys. **38**, 272–282 (2011).
[42]A. Partanen, P. S. Yarmolenko, A. Viitala, S. Appanaboyina, D. Haemmerich, A. Ranjan, G. Jacobs, D. Woods, J. Enholm, B. J. Wood, and M. R. Dreher, "Mild hyperthermia with magnetic resonance-guided high-intensity focused ultrasound for applications in drug delivery," Int. J. Hyperthermia **28**, 320–336 (2012).
[43]J. K. Enholm, M. O. Köhler, B. Quesson, C. Mougenot, C. T. Moonen, and S. D. Sokka, "Improved volumetric MR-HIFU ablation by robust binary feedback control," IEEE Trans. Biomed. Eng. **57**, 103–113 (2010).
[44]H. T. O'Neil, "Theory of focusing radiators," J. Acoust. Soc. Am. **21**, 516–526 (1949).
[45]F. A. Duck, *Physical Properties of Tissue: A Comprehensive Reference Book* (Academic Press Inc., San Diego, CA, 1990).
[46]S. A. Goss, R. L. Johnston, and F. Dunn, "Comprehensive compilation of empirical ultrasonic properties of mammalian tissues," J. Acoust. Soc. Am. **64**, 423–457 (1978).
[47]J. W. Valvano, "Tissue Thermal Properties And Perfusion," in *Optical-Thermal Response of Laser-Irradiated Tissue*, edited by A. J. Welch *et al.* (Springer, Dordrecht, the Netherlands, 2011).
[48]H. H. Pennes, "Analysis of tissue and arterial blood temperatures in the resting human forearm," J. Appl. Physiol. **1**, 93–122 (1948).
[49]I. Dragonu, P. L. de Oliveira, C. Laurent, C. Mougenot, N. Grenier, C. T. Moonen, and B. Quesson, "Non-invasive determination of tissue thermal parameters from high intensity focused ultrasound treatment monitored by volumetric MRI thermometry," NMR Biomed. **22**, 843–851 (2009).
[50]IEC, "IEC/TS 61949 ed1.0; Ultrasonics—Field characterization—*In situ* exposure estimation in finite-amplitude ultrasonic beams" (IEC, Geneva, 2007).
[51]A. Partanen, C. Mougenot, and T. Vaara, "Feasibility of agar-silica phantoms in quality assurance of MRgHIFU," AIP Conf. Proc. **1113**, 296–300 (2009).
[52]A. Ranjan, G. C. Jacobs, D. L. Woods, A. H. Negussie, A. Partanen, P. S. Yarmolenko, C. E. Gacchina, K. V. Sharma, V. Frenkel, B. J. Wood, and M. R. Dreher, "Image-guided drug delivery with magnetic resonance guided high intensity focused ultrasound and temperature sensitive liposomes in a rabbit Vx2 tumor model," J. Controlled Release **158**, 487–494 (2012).
[53]G. ter Haar, A. Shaw, S. Pye, B. Ward, F. Bottomley, R. Nolan, and A. M. Coady, "Guidance on reporting ultrasound exposure conditions for bio-effects studies," Ultrasound Med. Biol. **37**, 177–183 (2011).
[54]S. A. Sapareto and W. C. Dewey, "Thermal dose determination in cancer therapy," Int. J. Radiat. Oncol. Biol. Phys. **10**, 787–800 (1984).
[55]A. D. Maxwell, G. Owens, H. S. Gurm, K. Ives, D. D. Myers, Jr., and Z. Xu, "Noninvasive treatment of deep venous thrombosis using pulsed ultrasound cavitation therapy (histotripsy) in a porcine model," J. Vasc. Interv. Radiol. **22**, 369–377 (2011).
[56]C. C. Coussios, C. H. Farny, G. T. Haar, and R. A. Roy, "Role of acoustic cavitation in the delivery and monitoring of cancer treatment by high-intensity focused ultrasound (HIFU)," Int. J. Hyperthermia **23**, 105–120 (2007).
[57]P. R. Patel, A. Luk, A. Durrani, S. Dromi, J. Cuesta, M. Angstadt, M. R. Dreher, B. J. Wood, and V. Frenkel, "*In vitro* and *in vivo* evaluations of increased effective beam width for heat deposition using a split focus high intensity ultrasound (HIFU) transducer," Int. J. Hyperthermia **24**, 537–549 (2008).
[58]N. M. Hijnen, E. Heijman, M. O. Köhler, M. Ylihautala, G. J. Ehnholm, A. W. Simonetti, and H. Grull, "Tumour hyperthermia and ablation in rats using a clinical MR-HIFU system equipped with a dedicated small animal set-up," Int. J. Hyperthermia **28**, 141–155 (2012).
[59]D. L. Miller and C. Dou, "The potential for enhancement of mouse melanoma metastasis by diagnostic and high-amplitude ultrasound," Ultrasound Med. Biol. **32**, 1097–1101 (2006).
[60]G. O. Oosterhof, E. B. Cornel, G. A. Smits, F. M. Debruyne, and J. A. Schalken, "The influence of high-energy shock waves on the development of metastases," Ultrasound Med. Biol. **22**, 339–344 (1996).
[61]D. L. Miller, C. Dou, and J. Song, "Lithotripter shockwave-induced enhancement of mouse melanoma lung metastasis: Dependence on cavitation nucleation," J. Endourol. **18**, 925–929 (2004).
[62]K. Hynynen, "The threshold for thermally significant cavitation in dog's thigh muscle *in vivo*," Ultrasound Med. Biol. **17**, 157–169 (1991).
[63]M. J. Voogt, H. Trillaud, Y. S. Kim, W. P. Mali, J. Barkhausen, L. W. Bartels, R. Deckers, N. Frulio, H. Rhim, H. K. Lim, T. Eckey, H. J. Nieminen, C. Mougenot, B. Keserci, J. Soini, T. Vaara, M. O. Köhler, S. Sokka, and M. A. van den Bosch, "Volumetric feedback ablation of uterine fibroids using magnetic resonance-guided high intensity focused ultrasound therapy," Eur. Radiol. **22**, 411–417 (2012).
[64]S. Wang, V. Zderic, and V. Frenkel, "Extracorporeal, low-energy focused ultrasound for noninvasive and nondestructive targeted hyperthermia," Future Oncol. **6**, 1497–1511 (2010).